

Micro-Precision Interferometer: Scoreboard on Technology Readiness for the Space Interferometer Mission

Renaud Goullioud, Frank G. Dekens and Gregory W. Neat

Jet Propulsion Laboratory, California Institute of Technology, CA 91009, Pasadena, USA

ABSTRACT

We investigate how the Space Interferometry Mission (SIM) will be able to meet some of its instrument astrometrics requirements. This paper describes a evaluation study that enables the validation of some requirements on vibration isolation solutions and active optical systems under dynamic conditions and with metrics that are representative of those expected on-orbit for SIM.

The procedure involves interfacing the isolator under evaluation to the Micro-Precision Interferometer testbed (MPI) and measuring the requisite disturbance transfer functions in six degrees of freedom. These transfer functions accurately depict the effectiveness of the vibration isolation system and the active optics system at achieving nanometer stabilization of the optical elements. Modeled reaction wheel disturbance profiles are then played through this family of measurements to predict the on-orbit performance in terms of the desired metric; optical pathlength change and tip/tilt jitter of the instrument as a function of wheel speed. Applying different norms to these performance functions, the performance metric is simplified to a single number.

Using the procedure, it is possible to simulate several operating modes of SIM. These modes include fringe tracking, internal path stabilization and pointing. Each operating mode can be tested under various isolator configurations: hard mounted (no isolation), active hexapod isolator and perfect isolator (noise floor). The paper describes the various operating configurations, summarizes the test procedure, presents a description of each isolator configuration and lists the corresponding results from the evaluation analysis.

Keywords: Interferometry, Micro-Precision Interferometer, SIM

1. INTRODUCTION

Spaceborne optical interferometers use an array of two or more small telescopes, as opposed to a single large telescope, to collect light from a single target star. The light from these telescopes, or sub-apertures, is combined to create an interference fringe pattern. This pattern (optical path difference), which results when the distances from the observed star through each arm of the interferometer to the detector are equal, must be stabilized to the 10 nanometer level for successful instrument operation.¹

The Stellar Interferometer Mission (SIM) is a first-generation spaceborne interferometer concept with astrometric and imaging goals.² Unlike ground-based interferometers bolted to bedrock,³ instrument optics of SIM are distributed across a 10 m, light-weight structure. The primary mechanical disturbance sources exciting the structure are expected to be the spinning reaction wheels used as actuators for the attitude control system.

Simulation results suggest that in the unattenuated spacecraft environment, the optical path (fringe position) variation is a factor of one hundred above the 10 nm requirement.⁴ This discrepancy inspired the layered vibration attenuation control strategy which involves the blending of vibration isolation, structural quieting, and active optical control.⁵ This paper discusses vibration isolation and active optical systems. The isolator must isolate the vibrating reaction wheel payload from the quiet structure which supports the optical elements. The isolation system is particularly important in two interferometer operating modes; initial fringe acquisition and tracking. During fringe acquisition, the unacquired fringe position must be stable to 40 nm (MAX) for successful acquisition. The vibration

Other author information: (Send correspondence to Gregory W. Neat)

Gregory W. Neat: E-mail: neat@huey.jpl.nasa.gov

Renaud Goullioud: E-mail: renaud@huey.jpl.nasa.gov

Frank G. Dekens: E-mail: fdekens@huey.jpl.nasa.gov

attenuation strategies available during this mode are the vibration isolation system and optical systems which rely on metrology signals (as opposed to true star light). During tracking, the fringe position must be stable to 10 nm (MAX). However in this case, the vibration attenuation suite is increased to include the optical systems closed loop on the actual stellar signal.

This paper uses a performance evaluation procedure that enables the comparison of different vibration isolation solutions and active optical systems under dynamic conditions and with metrics that are representative of those expected on-orbit for spaceborne interferometers. Traditionally, performance assessment of vibration isolation systems has been done by measuring transmissibility from the noisy side to the quiet side on a test bench.⁶ When the base or the payload experience flexibility, this approach becomes extremely complex to interpret. In addition, although this strategy provides a quantitative technique for assessing isolator performance on its own, the mechanical boundary conditions are not representative of the on-orbit boundary conditions and it is difficult to extrapolate from the transmissibility results to actual instrument performance, especially in six axes.

First, the paper describes the various SIM operating configurations under test in this study. We also describe the MPI testbed used in the analysis. Then, the test procedure and the three isolator configurations are summarized. Finally, we display some measured and predicted plots and list the corresponding results from the evaluation procedure.

2. SIM TECHNOLOGY READINESS VERIFICATION

The Interferometry Technology Program is working on solving the technical challenges associated with SIM. In order to establish a precise connection between the Technology Program and the Flight team, a list of requirements has been defined, called TRDV for SIM Technology Readiness Verification. In practice, the TRDV matrix lists the SIM requirements and maps them to the Technology program objectives. Each entry of the TRDV is associated with a testbed capable of assessing the requirement.

The TRDV can be divided into two categories: the nanometer regime and the picometer regime. The picometer program assesses the optical quality of the interferometer, the performance of the metrology system, the thermal issues. The nanometer program will assess the control of the actuators of the interferometer. In particular, MPI is responsible for the validation of several requirements of the nanometer program. Table 1 lists the requirements assessed by MPI.

TRDW Entry	Sensor	Requirement	Servo	Bandwidth	Isolation
Guide OPD (A.3.1.1)	OPD	10 nm	Fringe tracker	100 Hz	Hexapod
Acquisition OPD (A.2.1.1)	OPD	40 nm	Delay line	700 Hz	Hexapod
Science OPD (A.4.1.1)	OPD	10 nm	Delay line	700 Hz	Hexapod
Nulling OPD (D.4.1)	OPD	1 nm	Delay line	700 Hz	Hexapod
Guide Tip/tilt (A.7.1.1)	camera	30 mas	Pointing	100 Hz	Hexapod
Science Tip/tilt (A.8.1.1)	camera	30 mas	None		Hexapod
Beam Walk (B.3.2.1.1.1)	PSD	100 mas	None		Hexapod

Table 1. Summary of TRDW requirement entries and MPI tests.

For the tests listed in Table 1, an isolator attenuates the disturbance from the reaction wheels. The final isolator configuration for SIM is not known yet, however a passive hexapod isolator is currently baselined for SIM. Reference¹³ presents an isolator trade study done on MPI.

2.1. Guide OPD

In the Guide OPD tracking mode, the interferometer is looking at a relatively bright star. This allows to close a fast loop on the interference fringes that need to be stabilized. In practice, the “Fringe tracker servo” will have a 100 Hz bandwidth (unity gain cross-over) with a 40 dB/decade rejection before the cross-over. The requirement in the TRDV matrix for the “Guide” interferometer OPD jitter is 10 nm max.

2.2. OPD Acquisition

In the OPD acquisition mode, the instrument is searching for the fringes. There is a requirement to stabilize enough the optical path for a short period of time so that the fringes can be found. The "Fringe tracker servo" is opened loop since there is no fringes to track on yet. However, the internal metrology can be used to stabilize the internal path variation with the delay line. The requirement in the TRDV matrix for the OPD jitter during the acquisition sequence is 40 nm max for a duration of 10 milli-seconds.

2.3. Science OPD

In the Science OPD tracking mode, the interferometer is looking at a dim star, too faint to allow a fast fringe tracking. Therefore, alternative techniques are used to stabilize the fringes: Internal metrology servo to stabilize the internal pathlength between the fiducials, and Feed-forward of the external pathlength using the two "Guide" interferometers. The requirement in the TRDV matrix for the "Science" interferometer OPD jitter is 10 nm max.

2.4. Nulling OPD

In the Nulling OPD tracking mode too, the interferometer is looking at a dim star, too faint to allow a fast fringe tracking. Therefore, alternative techniques are used to stabilize the fringes: Internal metrology servo to stabilize the internal pathlength between the fiducials, and Feed-forward of the external pathlength using accelerometers mounted on the siderostat to monitor the fiducial motion. The requirement in the TRDV matrix for the Nulling interferometer OPD jitter is 10 nm max.

2.5. Guide Tip/tilt

In the Guide Tip/tilt control mode, the interferometer is looking at a relatively bright star. This allows us to close a fast pointing loop on the star spots in the camera. In practice, the "Pointing servo" has a 100 Hz bandwidth with a 40 dB/decade rejection before the cross-over. The requirement in the TRDV matrix for the "Guide" interferometer pointing jitter is 30 milli-arcseconds maximum.

2.6. Science Tip/tilt

In the Science Tip/tilt control mode, the interferometer is looking at a dim star, too faint to allow a fast pointing loop. Therefore, the alternative technique to stabilize the wavefront tilt is to use a beacon laser to attenuate the internal tip-tilt. The requirement in the TRDV matrix for the "Science" interferometer pointing jitter in the camera is 30 milli-arcseconds maximum.

2.7. Beam Walk

Beam walk of the metrology beam on an imperfect mirror will produce a small pathlength variation of the internal path of a few 100 picometers since the mirror cannot be considered flat to the sub-nanometer level. This effect will break the consistency between the starlight beam and the metrology beam at its center is lost. In particular, one concern is the starlight beam walk on the Fast Steering Mirror optics (FSM). The requirement in the TRDV matrix for the beam walk on the fast steering mirror is a maximum of 100 milli-arcseconds.

3. MPI DESCRIPTION

Central to this performance evaluation procedure is the Micro-Precision Interferometer (MPI) testbed.^{7,8} Figure 1 shows a bird's eye view of the MPI testbed. Located at the Jet Propulsion Laboratory, the testbed contains all the subsystems necessary to assess the effectiveness of the vibration attenuation technologies. These subsystems are: a softly suspended truss structure with mounting plates for subsystem hardware; a six-axis vibration isolation system which can support a reaction wheel assembly to provide a flight-like input disturbance source; a complete Michelson interferometer; internal and external metrology systems; and a star simulator that provides stellar input to the interferometer collecting apertures.

The 7 m x 7 m x 6.5 m truss structure is composed of drawn thin walled aluminum tubes. Six independent kinematically mounted interface plates are distributed across the structure to enable the mounting of the interferometer optical elements. The entire structure is suspended from the ceiling with a CSA passive/active pneumatic/electromagnetic suspension system. The rigid body suspension modes are all below 1 Hz and the first flexible

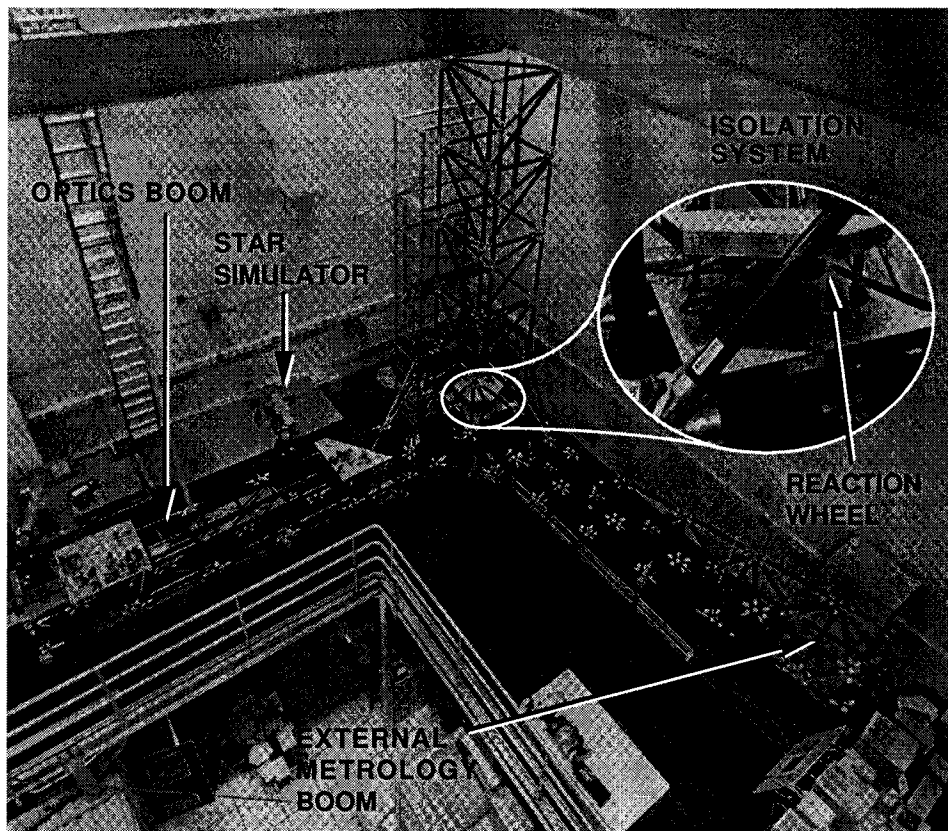


Figure 1. Bird's eye view of the MPI testbed with inset showing a close-up of the six-axis isolation system.

mode of the structure is just below 5 Hz. Further details on the structure design and assembly procedures are given in reference.⁹

Figure 2 shows the complete optical layout for the MPI Michelson interferometer and pseudo-star.¹⁰ The stellar source, a HeNe 633 nm laser, is located on a passively-isolated, four meter optical table. This beam is split and directed with flat mirrors to the respective testbed collecting apertures (or siderostat). Starting with each siderostat, the stellar light bounces off twelve surfaces (including the Fast Steering Mirror (FSM) and the delay lines) in each interferometer arm before recombining the two beams. After the beam combiner, the central portion of the combined stellar beams passes through the hole in an annular pick-off mirror to a fringe detector. The annular pick off mirror and subsequent folding mirrors reflect the outer annulus of each beam towards a high speed CCD camera.

In addition to the stellar beams, two independent internal metrology beams trace the internal paths of each interferometer arm (from the beam combiner to corner-cube retroreflectors at the center of the siderostats). The 1319 nm infrared metrology beam are injected at the center of the stellar beams through holes bored in fold mirrors.

3.1. Hexapod Isolation

Mechanical isolation is the first layer of rejection of the Reaction Wheel Assembly (RWA) disturbance. Close-up view in Figure 1 shows the hexapod isolator which interfaces to the structure via a 1 meter square plate, mounted to the flexible structure.

The hexapod system consists of six identical struts arranged in a mutually orthogonal configuration. Each of the isolator struts features a spring to provide axial compliance. The active isolator mode utilizes an active feedback loop on each strut. The active loop uses a voice coil electromagnetic actuator located inside the spring, acting in parallel with the spring and a force sensor for the feedback signal.

Although several hexapod isolators are available for MPI, this study was done with the active hexapod developed by TRW's Space & Electronics Group,¹¹ which is the most representative of the flight solution. The active loop

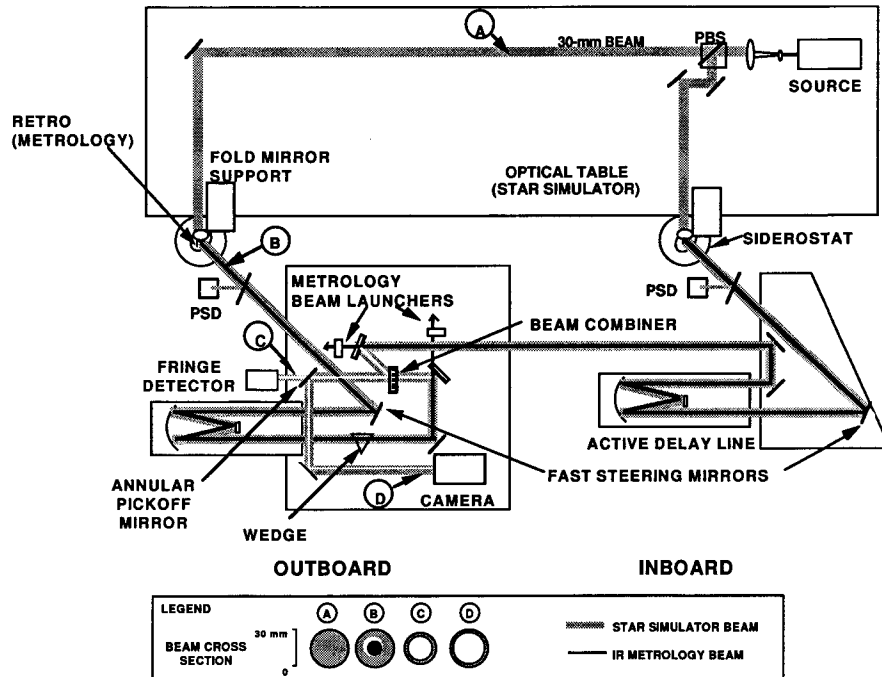
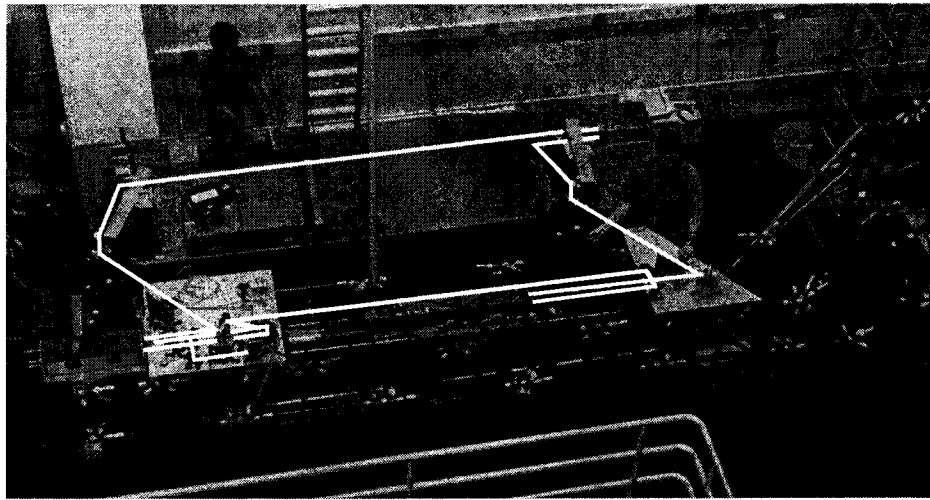


Figure 2. MPI optical layout. Both the block diagram and the photo depict the same region. Inset shows beam diameter at different locations.

augmented the existing passive isolation from 2 to 60 Hz with maximum feedback of 40 dB around 10 Hz. The active isolation modes of the hexapod are: 0.8 Hz for two lateral sway motions, 1.1 Hz for vertical bounce, 1.0 Hz for torsion and 2.8 Hz for the two rocking modes.

3.2. Fringe Tracker Servo

The interferometer must equalize the two optical paths (distance from the star, through each interferometer “arm” to the interference detector) to a small fraction of the wave length of light being observed (10 nm MAX). The active optics solution to this problem is to measure the Optical Path Difference (OPD) with the fringe detector (sensor) and subsequently introduce a delay into one of the interferometer “arms” to correct for the measured difference. This is done by linearly translating an optic called the delay line (actuator). Although the fringe detector actually measures the OPD at 4 kHz, the servo, called “fringe tracker” unity gain bandwidth is set at 100 Hz to match the predicted

observations. The Fringe sensor also provides the output signal (called "OPD") for the disturbance transfer function measurement procedure described in the following section.

3.3. Delay Line Servo

When Fringe tracking is not available, the internal metrology system can still be used to stabilize the internal pathlength changes. The active optics solution is to measure the internal path variation with the internal metrology system (sensor) and introduce a delay into one interferometer arm with the delay line (actuator). As the metrology runs at 4 kHz, the "Delay Line" servo bandwidth can be set at 700 Hz.

3.4. Guiding Servo

The pointing system of the interferometer must stabilize the tip/tilt of the star-light wavefront into the fringe detector to obtain a good fringe contrast (30 milli-arcseconds MAX). The active optics solution is to measure the tilt variation on the CCD camera (sensor) and to tilt the fast steering mirror (actuator) to cancel the measured wavefront tilt error. The laser beam is focused by a 1 meter focal length lens, to a location on the 32 by 32 pixel CCD camera. The digital image is processed in real-time at 4 kHz, in order to find the centroid of the beam images.¹² The centroid deviation from the target position is the tip-tilt provides the error signal for the "Guiding" servo and the output signal for the disturbance transfer function measurement. The fast steering mirror, made of three piezo actuators, position the mirror, providing tip and tilt motion without introducing path length changes.

4. PREDICTED RESULTS

4.1. Performance prediction method

MPI on-orbit performance is evaluated by combining disturbance transfer functions measured on the testbed with an analytical disturbance model. This hybrid experimental/analytical procedure allows one to predict on-orbit performance over an entire range of disturbance conditions in an accurate, efficient manner.¹³ One set of transfer function measurements can be convolved analytically with any combination of speeds of the four reaction wheels which would reside on the isolated platform of the spacecraft. Figure 3 shows how the task of representing the on-orbit problem has been distributed between the hardware and analysis tools. The four steps which make up this procedure are:

(1) the analytical reaction wheel disturbance model; based on test data obtained from the Hubble Space Telescope (HST) flight units,⁸ the disturbance forces and torques are modeled as discrete harmonics of the reaction wheel speed.

(2) measuring disturbance transfer functions from shakers to optical sensor; an HP signal analyzer generates a broadband drive signal applied to two shakers at the reaction wheel mounting location. The dynamometer (force sensor) produces a signal proportional to the disturbance, sent to the analyzer as the input for the transfer function. This disturbance is attenuated by the isolator, propagates through the structure and finally rattles the optical elements. The signal from the optical sensor under test is sent to the HP analyzer as the output for the transfer function measurement.

(3) the physical performance prediction algorithm; using the measured transfer functions and the wheel model, the algorithm generates predicted power spectrum densities of the optical signal as a function of wheel speed.^{12,13}

(4) the calculation of output optical performance metrics, the RMS and the MAX value of the optical jitter over all reaction wheel speeds.

4.2. Disturbance Interface Conditions

Three different impedance configurations between the disturbance source and the structure supporting the interferometer were tested. Figure 4 shows these three test configurations. The connections ranged from no isolation (hard mount), isolation (active hexapod), to "perfect" isolation (disturbance suspended from ceiling). In each case, the isolator system under test is located between the base plate, rigidly mounted to the structure and the payload which supports the disturbance source (shakers).

(1) "Perfect" Isolator

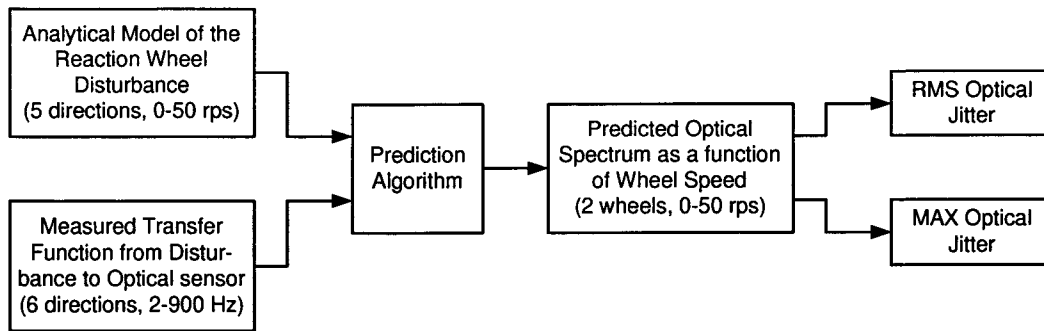


Figure 3. Isolator performance evaluation procedure.

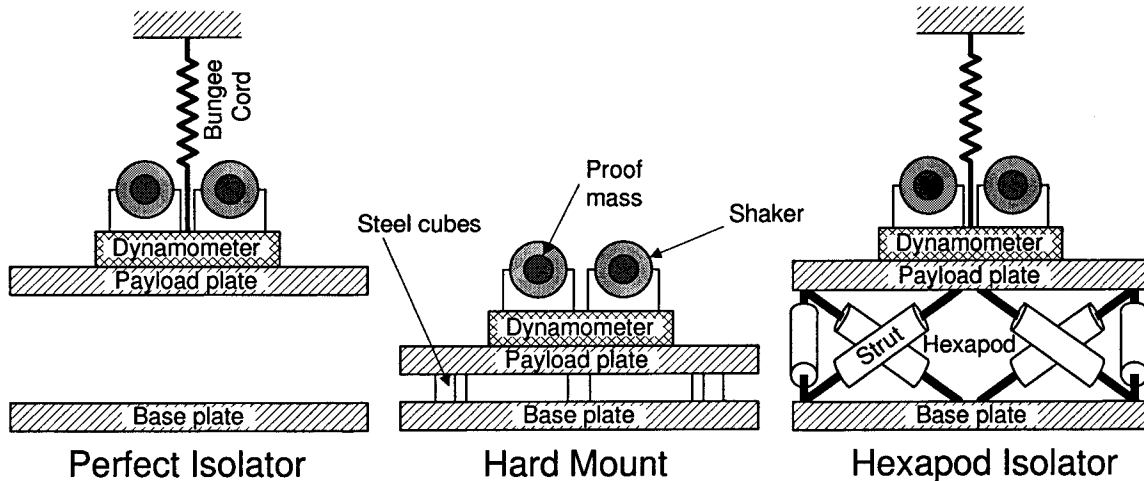


Figure 4. Test configurations used in this study.

The first configuration in Figure 4 was used to evaluate the performance of a “perfect” isolator in which there is no mechanical connection to the testbed. In this configuration, a bungee cord suspends the entire disturbance payload from the facility ceiling. Some of the subsequent configurations use the same bungee to minimize the effect of the 1-g gravitational sag on the isolator. The vertical resonant frequency of the suspended assembly was below 1 Hz and the lateral pendulum frequency was approximately 0.3 Hz

The test setup provides a means to quantify the noise floor of the transfer function measurement setup. The lab ambient disturbance environment, the data analyzer and testbed sensors all contribute to the transfer function noise floor. To demonstrate stabilization to the nanometer level requires a system with a noise floor below 1 nm.

(2) No Isolator (Hard Mounted)

To emulate the hard mounted disturbance configuration, the disturbance payload was bolted to the base plate through three steel cubes (second configuration of Figure 4). The three hard points were situated at the periphery of the payload plate, spaced 120° apart.

In contrast to the “perfect” isolator which provided a lower bound on the transfer function measurement setup, the hard mount configuration provides an upper bound to compare isolation system performance. Correspondingly, these two configurations bound the isolation performance metrics; the perfect isolator providing the lowest and the hard mounted providing the maximum metric values.

(3) Active Hexapod Isolator

The performance measurement procedure representative of the spacecraft isolator uses the active hexapod isolator described in the “MPI description” section (third configuration of Figure 4). Note on Figure 4 that the configuration utilizes the same off-load bungee used in the “perfect” isolator test. This is necessary since the passive isolator

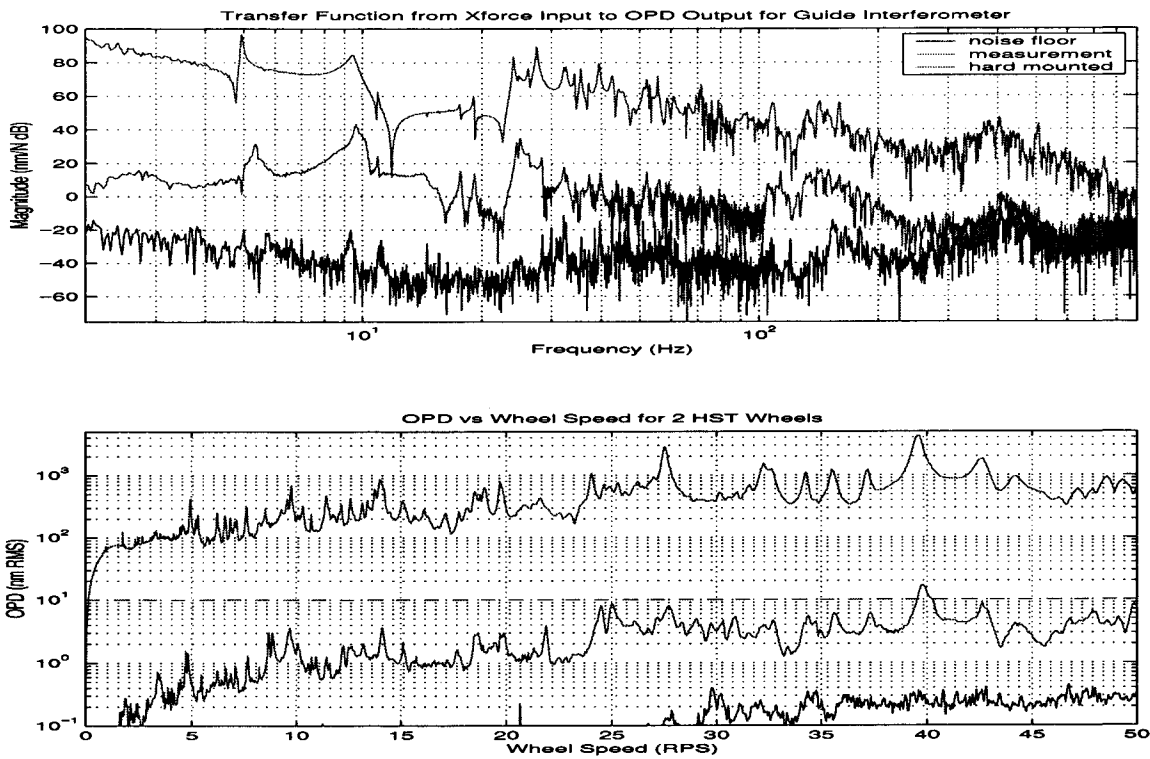


Figure 5. “Guide” OPD test - Top figure: OPD transfer functions for X force (from the top: hard mount, active hexapod isolator and perfect isolator) - Bottom figure: Predicted OPD as a function of RWA speed.

hexapod springs bottom out for a total vertical gravity load around 5 kg. In the space application the gravity effect will not be present.

4.3. Data Plots - Transfer Functions, OPD versus RPS Plots

A significant amount of data and processed data is associated with each test. For each test (check on Table 1), six disturbance transfer functions (one for each disturbance direction) are measured which constitute the input to the performance prediction algorithm. The algorithm output is two OPD (or Tip/tilt) versus wheel speed plots. Finally, two output performance metric values (RMS and MAX values) are generated from these four reaction wheel plots.

In the interest of brevity, just a few sample sets of disturbance transfer functions and reaction wheel OPD (or Tip/tilt) plots are shown. However, all of the output metrics for each test defined in Table 1 are tabulated in Table 2. Each sample set of plots (Figure 5 to 8) is shown for the active hexapod isolator configuration (the one representing SIM on-orbit conditions), in comparison with the hard mount (worst case) and the perfect isolator (noise floor). The upper plot presents one of the six measured disturbance transfer function while the lower plot presents the OPD (or tip/tilt) spectrum versus the wheel speed for two HST wheels.

(1) “Guide OPD” test

For this test, the “Fringe Tracker” servo is closed on the laser star. The servo has a unity gain cross-over at 100 Hz. The measured signal is the jitter of the servo. Figure 5 (top) shows the measured transfer functions for one direction (X disturbance force) of the “Guide” OPD test. The Fringe Tracker reduces response magnitude by 100 dB at low frequency, with diminishing returns above 100 Hz. The active hexapod isolator offers a reduction approaching 40 dB above 5 Hz compared to the hard mount. Together the fringe tracking servo and the active isolation reduce transmissibility significantly at any frequency.

Considering two reaction wheels, Figure 5 (bottom) shows the corresponding outputs from the performance prediction algorithm. Fringe tracking and active isolation succeeds in reducing response two orders of magnitude or more at any wheel speed, while the perfect isolator shows room for progress for at least another order of magnitude.

(2) “OPD Acquisition” test

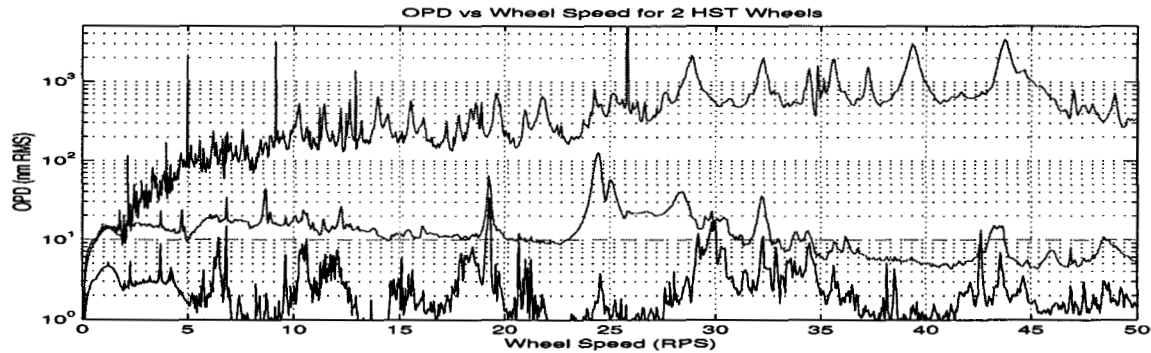
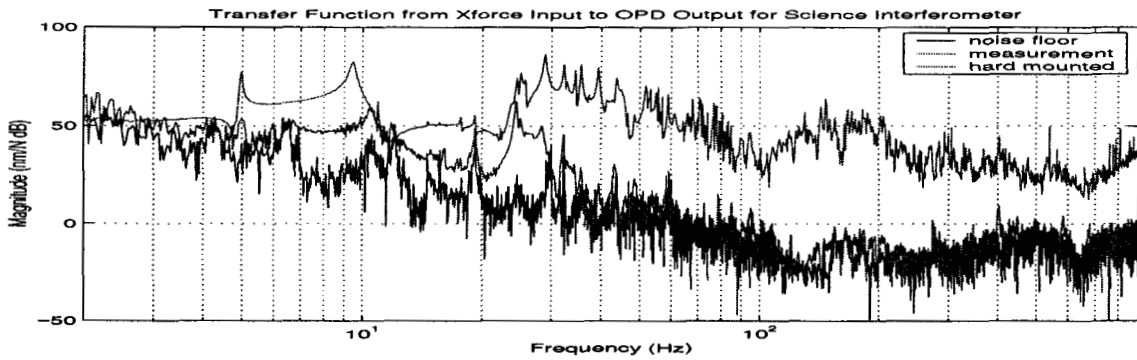


Figure 6. “Science” OPD test - Top figure: OPD transfer functions for X force (from the top: hard mount, active hexapod isolator and perfect isolator) - Bottom figure: Predicted OPD as a function of RWA speed.

For this test, the delay line servo is closed loop. The measured signal is the fringe position i.e. the full optical pathlength difference variation. The measured transfer functions are filtered prior to run the prediction algorithm to simulate 10 milliseconds of acquisition.

(3) “Science OPD” test

For this test, the “Delay Line” servo is closed on the internal laser metrology. The servo has a unity gain cross-over at 700 Hz. The Path Length Feed-Forward cannot be implemented on a simple baseline interferometer, therefore, the result of this test is a maximum value. The measured signal is the fringe position given by the “fringe tracker” in the opened loop mode.

Figure 6 shows one set of measured transfer functions and OPD versus wheel speed plots for the “science” OPD test. One can see that the Delay Line servo and the active isolation succeeds in reducing response one order of magnitude above 10 rps, and a further order of magnitude disturbance rejection above 35 rps.

(4) “Nulling” test

This test is identical to the “Science OPD” test. However we are currently testing accelerometers on the siderostat mounts.

(5) “Guide Tip/Tilt” test

For this test, the “Guiding” servo loop is closed on the position signal from the guiding camera signal using the FSM as an actuator. The servo has a unity gain cross-over at 100 Hz. The measured signal is the position jitter on the camera. Figure 7 shows one set of measured transfer functions and Tip/tilt versus wheel speed plots for the “Guide” Tip/tilt test. One can see that the Guiding servo and the active isolation succeeds in reducing response more than one order of magnitude at all wheel speeds.

(6) “Science Tip/Tilt” test

For this test, all servo are opened loop. The measured signal is the displacement of the laser-star spot on the guiding camera. Figure 8 shows one set of measured transfer functions and Tip/tilt versus wheel speed plots for

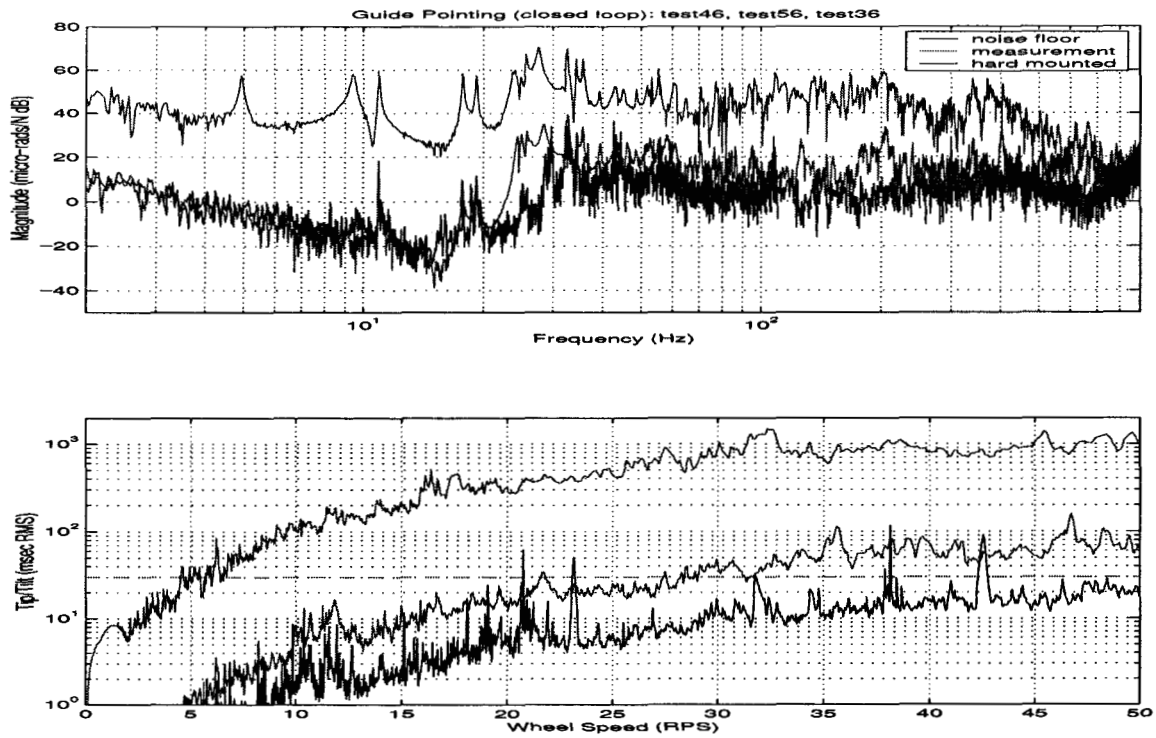


Figure 7. "Guide" Tip/tilt test - Top figure: tilt transfer functions for X force (from the top: hard mount, active hexapod isolator and perfect isolator) - Bottom figure: Predicted tilt as a function of RWA speed.

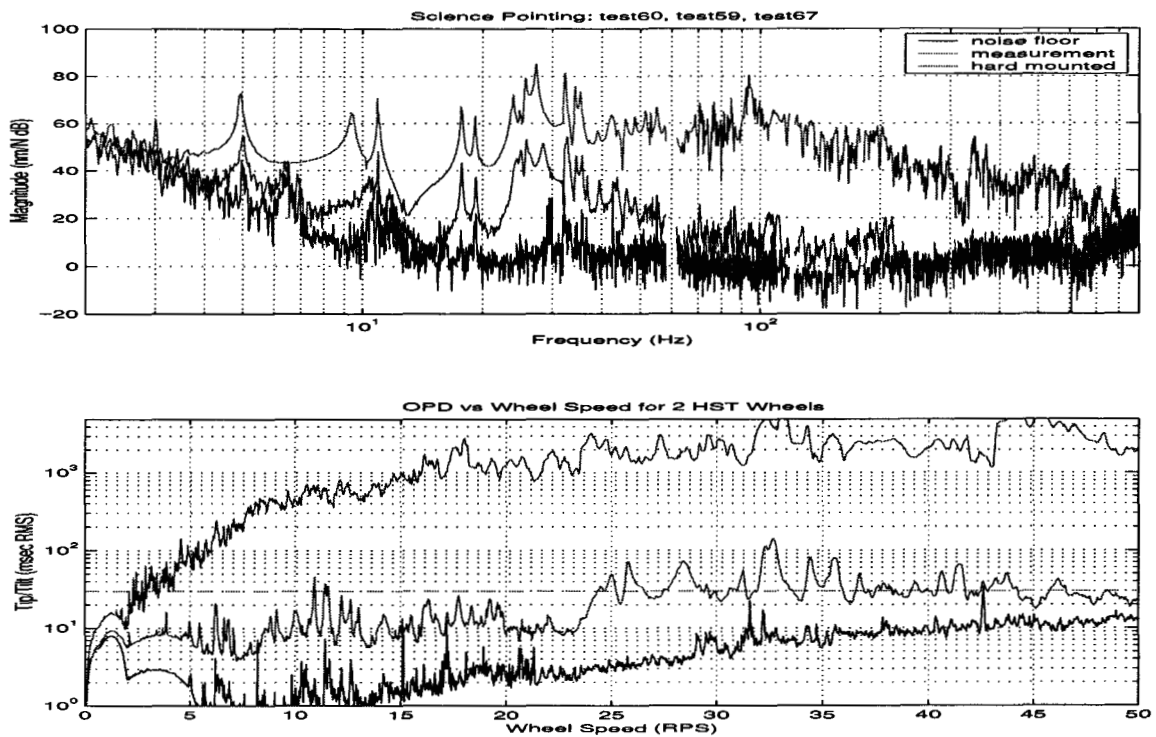


Figure 8. "Science" Tip/tilt test - Top figure: tilt transfer functions for X force (from the top: hard mount, active hexapod isolator and perfect isolator) - Bottom figure: Predicted tilt as a function of RWA speed.

the “Guide” Tip/tilt test. Although the no active optics are used, the active isolation alone succeeds in reducing response by one to two orders of magnitude above 10 rps.

(7) “Beam Walk” test

For this test, all servo are opened loop. The measured signal is the displacement of the laser-star spot on the PSD detector, just after the siderostats.

4.4. Score Card

Table 2 summarize all the previous tests; it is filled with the previously defined output metrics. These values, which are derived from the reaction wheel plots like in Figure 5, provide a quick mean of comparing the performance of testbed for each test with the requirements.

TRDW Entry	unit	Requirement	Measured RMS value	Measured MAX value	MAX/Req Ratio
Guide OPD (A.3.1.1)	nm	10	5.0	16.9	1.7
Acquisition OPD (A.2.1.1)	nm	40	22.1	61.7	1.5
Science OPD (A.4.1.1)	nm	10	25.8	126.8	12.7
Nulling OPD (D.4.1)	nm	1	25.8	126.8	127
Guide Tip/tilt (A.7.1.1)	mas	30	62.7	159.3	5.3
Science Tip/tilt (A.8.1.1)	mas	30	62.7	187.5	6.3
Beam Walk (B.3.2.1.1.1)	mas	100	30.0	99.9	1.0

Table 2. Summary of TRDW requirements and MPI results (given in nanometers (nm) and milli-arcseconds (mas)).

5. CONCLUSION/FUTURE WORK

This paper presents a prediction procedure to evaluate the performance of SIM on orbit. In practice, the SIM OPD and Tip/tilt tracking of the “Guide” and “science” conditions can be simulated. The resulting quantified performance values (Table 2) can be compared with the requirements issued from the SIM Technology Readiness table.

One must be careful with these numbers as MPI is slightly different from SIM. The HST wheel model has been created from table-top measurements; current test we a real reaction on the testbed will reduce the incertitude due to the boundary conditions. However, tests on MPI can give us very useful information for SIM: For example, they show that using passive isolation rather than active isolation will increase by a factor of 3 the measured numbers in Table 2. Also, using the Teledix reaction wheel rather than the HST wheel will double the measured numbers in Table 2.

Further tests include adding the siderostat accelerometers for the nulling OPD test, switching to 10 times beam compressors and reaction wheel validation.

ACKNOWLEDGMENTS

The research described was performed at the Jet Propulsion Laboratory of the California Institute of Technology, under contract with the National Aeronautics and Space Administration. The authors thank Rob Calvet and Jim Melody for their extensive contributions to the effort and the leaders of the Interferometer Technology Program, Bob Laskin, Jeffrey Yu, and Ben Parvin for their technical and financial support. The active/passive hexapod vibration isolator was developed and tested using TRW Independent Research and Development funds.

REFERENCES

1. M. M. Colavita, M. Shao, and M. D. Rayman, "OSI: Orbiting stellar interferometer for astrometry and imaging," in *Special Section on the Williamsburg Space Optics Conference*, 1991.
2. M. Shao and D. M. Wolff, "Orbiting stellar interferometer," in Reasenberg,¹⁴ pp. 228–239.
3. M. Shao, M. M. Colavita, B. E. Hines, D. H. Staelin, D. J. Hutter, K. J. Johnston, D. Mozurkewich, R. S. Simon, J. L. Hersey, J. A. Hughes, and G. H. Kaplan, "Mark III stellar interferometer," *Journal of Astronomy and Astrophysics* **193**, pp. 357–371, 1988.
4. R. A. Laskin and A. M. San Martin, "Control/structure system design of a spaceborne optical interferometer," in *Proc. AAS/AIAA Astrodynamics Specialist Conference*, (Stowe, VT), Aug. 1989.
5. J. T. Spanos, Z. Rahman, C.-C. Chu, and J. F. O'Brien, "Control structure interaction in long baseline space interferometers," in *Proc. 12th IFAC Symposium on Automatic Control in Aerospace*, (Ottobrunn, Germany), Sept. 1992.
6. J. T. Spanos, Z. Rahman, and G. H. Blackwood, "A soft 6-axis active vibration isolator," in *Proc. American Control Conference*, (Seattle, WA), June 1995.
7. G. W. Neat, J. F. O'Brien, N. M. Nerheim, R. J. Calvet, H. Singh, and S. Shaklan, "Micro-precision interferometer testbed: First stabilized stellar fringes," in Reasenberg,¹⁴ pp. 104–115.
8. G. W. Neat, A. Abramovici, J. W. Melody, R. J. Calvet, N. M. Nerheim, and J. F. O'Brien, "Control technology readiness for spaceborne optical interferometer missions," in *Proc. Space Microdynamics and Accurate Control Symposium*, (Toulouse, France), May 1997.
9. L. F. Sword and T. G. Carne, "Precision truss structures from concept to hardware reality: Application to the micro-precision interferometer testbed," in *Spaceborne Interferometry*, R. D. Reasenberg, ed., vol. 1947 of *Proc. SPIE*, pp. 104–113, (Orlando, FL), Apr. 1993.
10. G. W. Neat, J. W. Melody, and B. J. Lurie, "Vibration attenuation approach for spaceborne optical interferometers," *IEEE Transactions on Control Systems Technology* **6**, pp. 689–700, November 1998.
11. T. W. Nye, A. J. Bronowicki, R. A. Manning, and S. S. Simonian, "Applications of robust damping treatments to advanced spacecraft structures," in *Guidance Navigation and Control Conf.*, (Breckenridge, CO), 1997.
12. F. G. Dekens and G. W. Neat, "Micro-precision interferometer: Pointing system performance in on-orbit disturbance environment.," in *Proc. SPIE Conference on Smart Structures and Integrated Systems*, vol. 3668, pp. 426–439, Mar. 1999.
13. J. F. O'Brien, R. Goullioud, and G. W. Neat, "Micro-precision interferometer: Evaluation of new disturbance isolation solutions," in *Proc. SPIE Conference on Passive Damping and Isolation*, vol. 3327, (San Diego, CA), Mar. 1998.
14. R. D. Reasenberg, ed., *Spaceborne Interferometry II*, vol. 2447 of *Proc. SPIE*, (Orlando, FL), Apr. 1995.